

---

*Research article*

## Exploring large pore size alumina and silica-alumina based catalysts for decomposition of lignin

Sara Pourjafar<sup>1</sup>, Jasmine Kreft<sup>1</sup>, Honza Bilek<sup>2</sup>, Evguenii Kozliak<sup>2</sup> and Wayne Seames<sup>1,\*</sup>

<sup>1</sup> Chemical Engineering Department, University of North Dakota, Grand Forks, ND, USA

<sup>2</sup> Department of Chemistry, University of North Dakota, Grand Forks, ND, USA

\* **Correspondence:** Email: wayne.seames@ndus.edu; Tel: +17017772958.

**Abstract:** Evaluation of copper doped silica-alumina and  $\gamma$ -alumina catalysts for lignin decomposition was conducted using a suite of chemical analysis protocols that enabled a comprehensive characterization of the reaction product. X-ray diffraction analysis was used to verify the concentration of doped copper on catalyst supports. Then, batch experiments were performed to study the significance of catalyst support type, catalyst dopant concentration, lignin concentration, catalyst-to-lignin ratio, reactor stirring rate and reaction time. Aqueous products were extracted with dichloromethane and analyzed using a detailed gas chromatography-mass spectrophotometry analytical protocol, allowing for quantification of over 20 compounds. Solid residues were analyzed by thermogravimetric analysis and scanning electron microscopy. The highest yield of monomeric products from these screening experiments occurred with 5 wt% Cu on silica-alumina with a 1:1 w/w ratio of catalyst to lignin. A second set of experiments were conducted at these conditions to evaluate the effect of varying the reaction temperature between 300 and 350 °C. Lower reaction temperatures (300 °C) resulted in more unreacted lignin while higher temperatures (>350 °C) led to an increased formation of liquid phase products, but also increased char formation. While the total amount of liquid phase products increased, the combined yield of monomer phenolic products was only 5–7 wt% of the liquid extracted product and statistically independent of temperature and other operational parameters, although the yields of different chemicals varied with temperature. Unlike most pyrolytic processes, the concentration of gas phase products gradually decreased with increasing reaction temperature and became negligible at 400 °C, while the formation of coke increased with temperature. This seemingly contradictory result is likely due to increased product polymerization occurring at higher temperatures.

**Keywords:** lignin decomposition; doped catalysis; renewable fuels; renewable chemicals; zeolyte

## 1. Introduction

Lignocellulosic feedstock is well known as a renewable source of biofuels. This resource is attractive because it does not compete directly with edible plant production. However, most current biomass conversion processes only use cellulose and hemicellulose, leaving lignin behind as a low-grade boiler fuel feedstock. The ability to generate higher value fuel and chemical intermediates from this lignin would increase the economic attractiveness of lignocellulosic biofuel facilities.

Lignin is a complex three-dimensional polymer, which is rich in aromatic phenolic units. Cross-linkages within lignin provide structural stability to plants but also hinders decomposition. Furthermore, lignin isolation from plant biomass by most of the available industrial methods, e.g., obtaining Kraft lignin, was recently shown to replace ether phenolic unit links, particularly the most abundant  $\beta$ -O-4 bonds, into much more recalcitrant C-C bonds [1–5].

Various lignin degradation methods such as pyrolysis, acidolysis, hydrogenolysis, enzyme-based oxidation, etc., have been proposed [6–8]. Lignin thermal decomposition products are typically separated into four primary fractions: aqueous distillate, tar, gaseous products and coke [9]. The aqueous distillate typically includes groups of products such as cresols, catechols, vanillin and guaiacols, which are difficult to obtain from a single step petrochemical process and thus have potential as valuable chemical or fuel intermediates [10].

Table 1 provides a summary of representative previous studies where heterogeneous acids were used to facilitate the decomposition of lignin. This information, given the variation in reaction conditions and analytical protocols (as well as hydrogen generation when using tetralin or formic acid), suggests that more sophisticated acid catalysts may show greater promise than simple inorganic acids. Among well-known commercially available acidic catalysts, zeolites present an attractive option as they are able to degrade a variety of biomass feedstocks into mixtures of aromatics [11]. Zeolites are composed of a silica and alumina tetrahedral network. Their microporous structure allows small reactants to diffuse into the crystal where many active acidic sites are located [12]. However, the comparison provided in Table 1 shows that one of the major drawbacks of using zeolites to degrade processed lignin is the significant amount of char that forms on or within the zeolite's structure. Char fouls the catalyst and may make its regeneration expensive or even infeasible.

**Table 1.** Representative previous studies of heterogeneous acid catalyzed degradation of lignin.

Catalyst	Feedstock	Reaction condition	Products	Reference
H <sub>2</sub> O-CO <sub>2</sub>	Alkali lignin	200–500 °C, water, 10 min	30% phenolic organic products at 350 °C	[13]
Si-Al cat ZrO <sub>2</sub> -Al <sub>2</sub> O <sub>3</sub> -FeO <sub>x</sub>	Kraft lignin	200–350 °C, water/butanol, 2 h	6.5% phenols	[14]

*Continued on next page*

Catalyst	Feedstock	Reaction condition	Products	Reference
ZSM-5, $\beta$ -zeolite, Y-zeolite	Lignin extracted from pulp mill black liquor	Fast pyrolysis, 650 °C, helium flow	Increasing the $\text{SiO}_2/\text{Al}_2\text{O}_3$ ratio in zeolites structure decreased the aromatic yield	[15]
$\text{Mo}_2\text{N}/\gamma\text{-Al}_2\text{O}_3$	Alkaline lignin	500–850 °C, fast pyrolysis, helium flow	Presence of $\text{Mo}_2\text{N}/\gamma\text{-Al}_2\text{O}_3$ decreased oxygenated volatile organics and increased aromatic hydrocarbons (mostly benzene and toluene)	[16]
HZSM-5: $\text{SiO}_2/\text{Al}_2\text{O}_3 = 25\text{--}200$	Alkaline lignin	500–764 °C, 3–99 sec, helium flow	Aromatics increased from 0.2 to 5.2 wt% while coke also increased from 24 to 39.7%	[17]
Formic acid, Pd/C, Nafion SAC-13	Kraft spruce	300 °C, water	Guaiacol, pyrocatechol and resorcinol as main phenols	[18]
$\text{ZrO}_2 + \text{K}_2\text{CO}_3$	Kraft lignin	350 °C, phenol/water	Presence of $\text{K}_2\text{CO}_3$ increased the formation of 1-ring aromatic products from 17% to 27%	[19]
Ni-Mo/ $\text{Al}_2\text{O}_3$	Wheat straw soda lignin	350 °C, tetralin, 5 h	Lignin was converted into gases (9 wt%) and liquids (65 wt%)	[20]
$\text{MoS}_2$	Kraft lignin	400–450 °C, 1 h, water	Phenols (8.7% of the original lignin), cyclohexanes (5.0%), benzenes (3.8%), naphthalenes (4.0%), and phenanthrenes (1.2%) were produced	[21]

Hydrogenated Zeolite Socony Mobil-5 (H-ZSM-5) has a higher density of both Brønsted and Lewis acid sites (related to the activity of many catalysts in C-C cleavage reactions) compared to most commercially available catalysts [22]. However, this does not necessarily mean that higher catalyst acidity will result in higher conversion of lignin to low molecular weight compounds as the small pore size limits catalytic activity to secondary reactions [23]. The zeolite pore size is usually around 2–4 nm while silica-alumina catalysts have a pore diameter of around 8 nm, which may be more appropriate for degradation of large polymer lignin molecules or oligomeric intermediates formed as a result of prior thermal decomposition of this feedstock.

A comparison of amorphous  $\text{SiO}_2\text{-Al}_2\text{O}_3$  catalysts to various types of zeolites shows that amorphous  $\text{SiO}_2\text{-Al}_2\text{O}_3$  has a lower surface area than HZSM-5, Y-zeolite or  $\beta$ -zeolite [24]. However, amorphous  $\text{SiO}_2\text{-Al}_2\text{O}_3$  has the largest pore volume, which is around 0.75 mL/g. Either lignin macromolecules or oligomeric intermediates of primary reactions may diffuse into these large pores, allowing the catalyst to participate in either primary or secondary degradation reactions. By contrast, smaller pore size zeolites are likely only facilitating either secondary or even further subsequent reactions. Lignin's recalcitrance toward degradation suggests that enhancing the primary decomposition reactions may increase the yield of the most valuable degradation products, e.g., organic monomers and dimers.

Therefore, in this study, catalytic thermal degradation of lignin was investigated using silica-alumina and  $\gamma$ -alumina catalyst supports. We postulated 1) that the use of catalysts with a pore

size larger than that of zeolites might enhance the targeted catalytic activity and 2) that a similar, potentially synergetic effect would be achieved while using a copper dopant. Previous research has shown that Cu-doped catalysts not only improved the physical strength of the catalyst under hydrotreatment conditions, but also deoxygenated lignin model compounds [28]. Preliminary tests (results not shown) also identified copper from a suite of potential metal dopants as the most attractive additive to promote lignin decomposition into monomer and dimer products. Screening was conducted to examine the effect of the catalysts and operating conditions on final products yield and composition. This was followed by a parametric study to determine the optimum reaction temperature. The application of detailed chemical analysis protocols resulted in a comprehensive characterization of the reaction products.

## 2. Materials and method

### 2.1. Materials

Indulin AT (softwood lignin commercialized in Kraft form), was supplied by MeadWestvaco (Glen Allen, VA). Silica-alumina was purchased from Sigma-Aldrich (St. Louis, MO) and  $\gamma$ -alumina with a specific surface area of 255 m<sup>2</sup>/g and a total pore volume of 1.12 cm<sup>3</sup>/g was obtained from Alfa Aesar (Haverhill, MA) as 3 mm extruded granules.  $\gamma$ -alumina granules were crushed and sieved to 150  $\mu$ m particles. Copper (II) nitrate hemipentahydrate (Cu(NO<sub>3</sub>)<sub>2</sub> × 2.5H<sub>2</sub>O), and acetone ( $\geq$ 99.9% purity) were purchased from Sigma Aldrich (St. Louis, MO). Purified water was obtained from an in-house milli-Q ultrafiltration system and was used for catalyst preparation and degradation experiments.

### 2.2. Experimental methods

#### 2.2.1. Metal doped catalyst preparation

Before impregnation, SiO<sub>2</sub>-Al<sub>2</sub>O<sub>3</sub> and  $\gamma$ -alumina catalyst supports were calcined separately at 500 °C for 6 hours in a muffle furnace for complete transformation to their protonic forms. An aqueous colloidal solution with a defined quantity of Cu was added to a beaker containing activated SiO<sub>2</sub>-Al<sub>2</sub>O<sub>3</sub> or  $\gamma$ -alumina (depending on the catalyst being made). Each solution was stirred at room temperature overnight. The well-dispersed mixture was then placed in the furnace at 120 °C for 12 hours where all the water evaporated. The solid was crushed to fine powder and was again placed in the oven at 500 °C for 4 hours to complete the calcination process. X-ray diffraction (XRD) analysis was used to verify the concentration of doped copper on catalyst supports.

#### 2.2.2. Lignin decomposition experiments

All experiments were conducted in a 500 mL batch autoclave reactor purchased from Parr Instruments Company (Parr 4575 series HP/HT). A schematic diagram of the reactor is shown in Figure 1. Defined amounts of lignin, metal-doped catalyst and purified water were mixed in a beaker. To obtain a homogeneous suspension of water/lignin/catalyst, the beaker was placed in a sonicator for 30 minutes. The mixture was poured into the reaction vessel, which was then sealed. The reaction

vessel was purged three times with nitrogen in order to remove atmospheric gases. After purging the vessel, the reactor was charged for one last time with nitrogen to the reaction starting pressure.

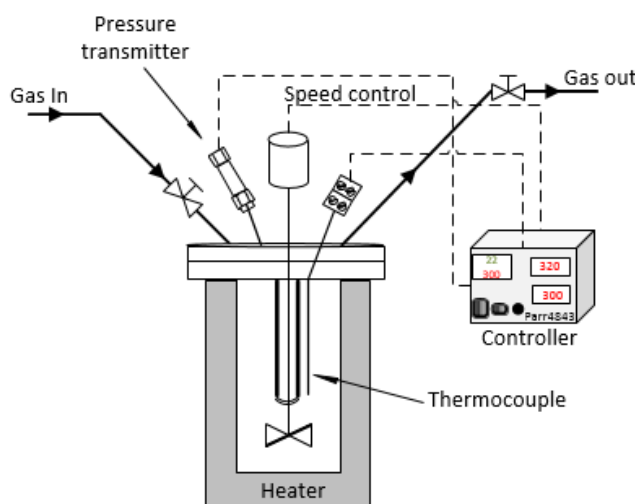


**Figure 1.** Schematic diagram of the batch reaction vessel used for all lignin decomposition experiments.

Depending on the desired reaction temperature, it took around 2 to 3.5 hours for the system to reach the target temperature. After completion of reaction, the vessel was cooled down by cold running water inside a coil inserted in the reactor. The system temperature returned to room temperature in approximately one hour. After cooling, gas was vented, and the mixture of liquid and solid products were separated using vacuum filtration. The reaction vessel was then washed with acetone to collect solid residues. Solid residues on the filter paper were recovered using acetone and dried at 80 °C for further gravimetric analysis.

### 2.2.3. Screening studies

A six-run Plackett-Burman design was used to screen the importance of six factors associated with catalyst synthesis and optimization of the reaction condition. Table 2 shows the experimental design with the selected factors at their low and high levels. The experiments were conducted in duplicate and each replicate was studied in a block. All the experiments in each replicate were randomized for screening the significant factors.

The first four factors presented in Table 2 were used to study the effects of the catalyst on lignin decomposition. The first factor listed is the catalyst support type. Amorphous silica-alumina is a commercially available catalyst for hydrocracking of heavy oil fractions [25]. Although the density of Brønsted acid sites in silica-alumina is not as high as in zeolites, silica-alumina catalysts have been shown to be very efficient at breaking strong C-C bonds compared to zeolites and clay [26]. As discussed in the introduction, we postulate that their microporous structure will facilitate absorption and desorption of lignin and its primary decomposition products, which, as we postulated, increases production of the target liquid organic monomers while inhibiting catalyst fouling. This catalyst was compared to a  $\gamma$ -alumina catalyst with a pore size comparable to the amorphous silica-alumina.

Lewis acid sites in  $\gamma$ -alumina catalysts have been shown to be suitable for pre-cracking of hydrocarbon macromolecules [22]. The next factor listed in Table 2 examined the Cu dopant concentration. We also varied the lignin concentration in the water solvent and the lignin-to-catalyst ratio (LCR). The LCR factor examined the effect of acidic-site densities on the product composition.

**Table 2.** Values and experimental design for the six factors tested in screening study.

Run order	Catalyst support	Dopant concentration wt%	Lignin concentration (wt%)	Lignin-to-catalyst ratio (g/g)	Stirrer rate (rpm)	Reaction time (min)
1	Al <sub>2</sub> O <sub>3</sub>	5	1.7%	1	400	45
2	Al <sub>2</sub> O <sub>3</sub>	10	1.2%	1	400	30
3	SiO <sub>2</sub> /Al <sub>2</sub> O <sub>3</sub>	10	1.2%	1.5	400	45
4	SiO <sub>2</sub> /Al <sub>2</sub> O <sub>3</sub>	10	1.7%	1	320	30
5	Al <sub>2</sub> O <sub>3</sub>	5	1.2%	1.5	320	30
6	SiO <sub>2</sub> /Al <sub>2</sub> O <sub>3</sub>	5	1.7%	1.5	320	45
7	SiO <sub>2</sub> /Al <sub>2</sub> O <sub>3</sub>	5	1.7%	1.5	320	45
8	Al <sub>2</sub> O <sub>3</sub>	5	1.2%	1.5	320	30
9	Al <sub>2</sub> O <sub>3</sub>	10	1.2%	1	400	30
10	SiO <sub>2</sub> /Al <sub>2</sub> O <sub>3</sub>	10	1.2%	1.5	400	45
11	SiO <sub>2</sub> /Al <sub>2</sub> O <sub>3</sub>	10	1.7%	1	320	30
12	Al <sub>2</sub> O <sub>3</sub>	5	1.7%	1	400	45

The remaining factors tested reaction conditions by varying the stirring rate and the reaction time. Preliminary testing showed that at stirring rates below 320 rpm, mixing was inefficient and most of the lignin powder settled on the bottom of the vessel while at above 400 rpm a significant amount of char was generated due to the strong vortex that threw lignin powder out of the liquid phase. Although very short reaction times may result in incomplete degradation of lignin, long residence times may have negative effects such as re-polymerization and the formation of char and gaseous products. The factor values of 30 and 45 min were based on the time that passes after the vessel reaches the set temperature, ignoring initial heating time.

#### 2.3.4. Reaction temperature variation studies

The effect of temperature on lignin degradation was examined in more detail using the best set of conditions from the initial screening study. The reaction conditions for this temperature study are summarized in Table 3. Each experiment was conducted in triplicate.

**Table 3.** Conditions for the reaction temperature variation studies.

Reaction temperature	300, 320, 350 °C
Lignin concentration in water	1.2 wt%
Catalyst	5 wt% Cu in SiO <sub>2</sub> -Al <sub>2</sub> O <sub>3</sub>
Stirring rate	400 rpm
Reaction time	30 min

### 2.3.5. Characterization

Liquid-liquid extraction (LLE) using dichloromethane (DCM) was used to remove liquid phase lignin decomposition products from the resulting aqueous phase following the procedure designed by Voeller et al. [29]. 50  $\mu\text{L}$  of a recovery standard (4-chloroacetophenone) was added to 1.0 mL of a liquid sample to monitor the losses during the extraction. 1.0 mL of DCM was added and then the sample was vortexed for 1 minute. After separation of the DCM and water phases, the DCM layer was collected and transferred to a test tube. This process was repeated three times, resulting in 3 mL of DCM phase liquid. At the end, 75  $\mu\text{L}$  of an internal standard (o-terphenyl) was added to this organic phase (DCM) sample and injected into the GC-MS for analysis.

Analyses of lignin decomposition products were performed using a gas chromatography-mass spectrometer (GC-MS, HP 5890 gas chromatograph) equipped with an autosampler (HP 7673 injector). The analyses were performed in splitless mode with an injection volume of 1  $\mu\text{L}$ . GC separation was performed using a 42 m long Agilent DB-5MS capillary column with 250  $\mu\text{m}$  I.D. and 0.25  $\mu\text{m}$  film thickness. Helium was used as a carrier gas at a constant flow rate of 1.2 mL/min. The GC column temperature program started at 50  $^{\circ}\text{C}$  for 1 min, followed by a 40  $^{\circ}\text{C}/\text{min}$  gradient to 80  $^{\circ}\text{C}$ , a 25  $^{\circ}\text{C}/\text{min}$  gradient to 320  $^{\circ}\text{C}$ , and a hold for 7 min. The MS was used in the full scan mode ( $m/z$  of 33–700 amu) with the transfer line temperature of 280  $^{\circ}\text{C}$ . Quantification and identification of all samples were based on the corresponding standards.

Thermogravimetric analysis (TGA) of selected reactor solid residues was carried out using a TA Instruments TGA-DSC Q-series (SDT-Q600). Thermal gravimetric curves were obtained under a dynamic atmosphere of argon at a constant flow of 100 mL/min. The temperature program was as follows: isothermal at room temperature for 5 minutes, ramp with a heating rate of 25  $^{\circ}\text{C}$  per minute, then isothermal for 5 minutes at 300, 400, 500, 850 and 870  $^{\circ}\text{C}$ .

Scanning electron microscopy (SEM, Hitachi S-3400N equipped with high TOA ports for energy-dispersive spectroscopy [EDS], Japan) was employed to study the surface morphology of selected catalysts and reactor residues. All the samples were gold coated for 40 s.

The XRD analysis of the doped catalysts was conducted using a Rigaku Smartlab 3 Kw instrument equipped with a D/teX detector using Cu  $K\alpha$  radiation ( $\lambda = 1.5302 \text{ \AA}$ ). The samples were scanned in a range of  $2\theta$  between 10 and 80 $^{\circ}$ .

## 3. Results and discussion

### 3.1. Catalyst characterization

XRD profiles of silica-alumina and  $\gamma$ -alumina are presented in Figures 2a and b, respectively. As can be seen, characteristic peaks of copper showed up in both silica-alumina and  $\gamma$ -alumina catalyst supports, which verifies the success of the doping protocol. SEM analysis was performed to further characterize the catalysts. Results of SEM and EDS analyses of 5 wt% and 10 wt% copper doped silica-alumina are shown in Figure 3. As can be seen, copper was well-dispersed on the surface of the silica-alumina catalyst and its characteristic peak was identified in the EDS profile.

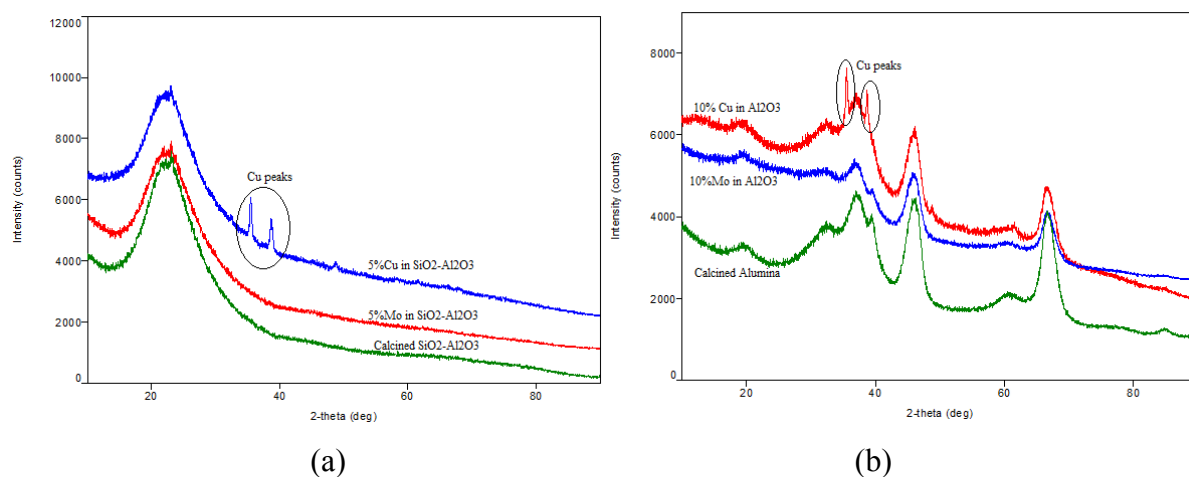


**Figure 2.** XRD patterns of calcined silica-alumina compared to Mo (blank) and completely undoped catalyst a) 5 wt% Cu on  $\text{SiO}_2/\text{Al}_2\text{O}_3$  and b) 10 wt% Cu on  $\gamma$ -alumina.

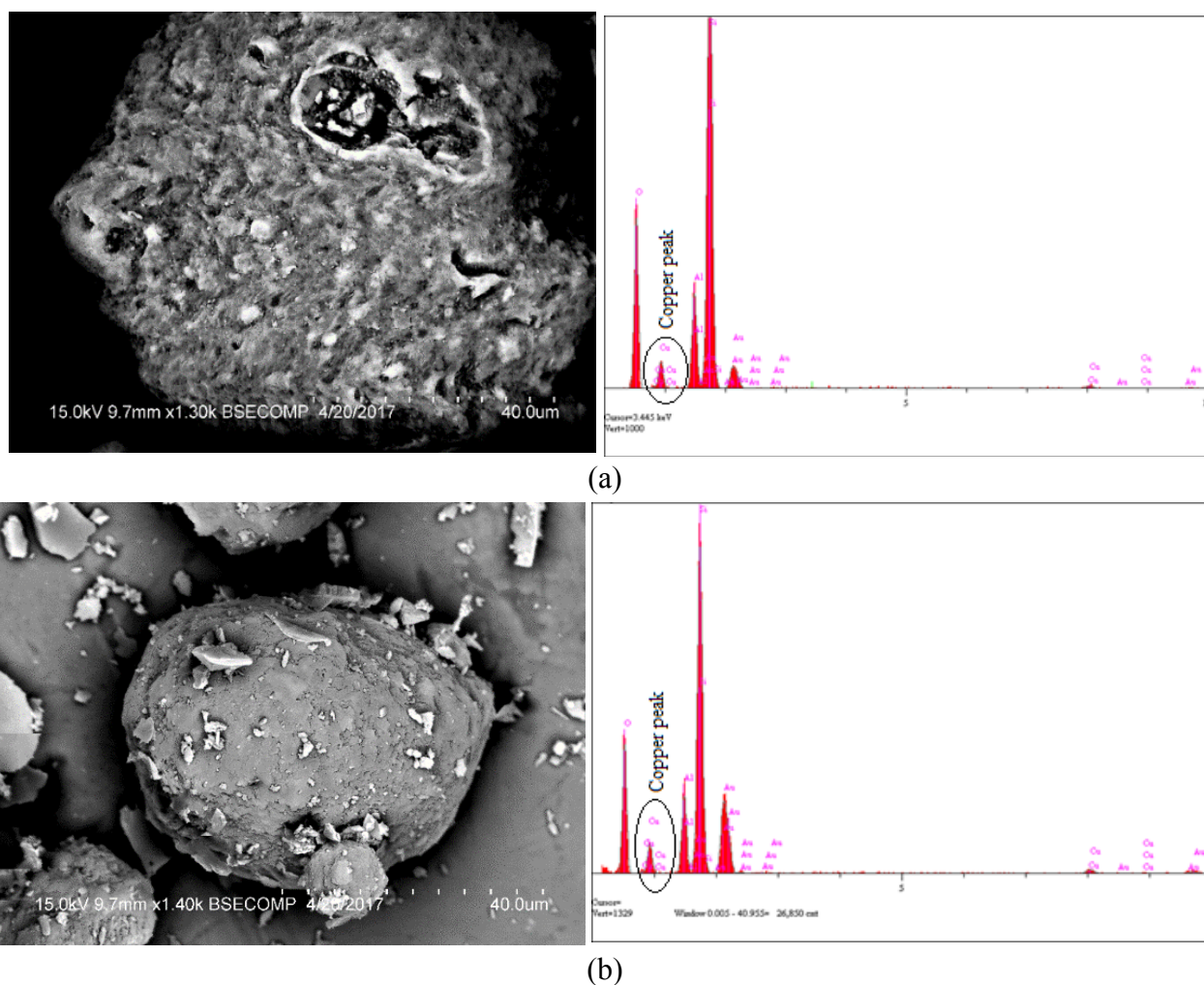


**Figure 3.** SEM and EDS analysis of a) 5 wt% Cu in  $\text{SiO}_2/\text{Al}_2\text{O}_3$  and b) 10 wt% Cu in  $\text{SiO}_2/\text{Al}_2\text{O}_3$ .



### 3.2. Screening study results

Table 4 summarizes the results obtained from GC-MS analysis of the liquid phase collected from the screening experiments. The identified compounds were lumped under five general categories: guaiacols, guaiacyl carbonyls, guaiacyl dimers, guaiacyl acids, and other compounds, which were mainly represented by syringol and homovanilyl alcohol. Individual chemical compositions are available in Pourjfar [30].

**Table 4.** Concentration of compounds (wt%) in the liquid product phase classified by product type.

Run	Guaiacols	Guaiacyl carbonyls	Guaiacyl dimers	Guaiacyl acids	Other	Total
1	1.1	1.1	0.1	2.6	2.6	7.5
2	0.6	1.2	0.0	2.6	3.0	7.3
3	1.3	1.4	0.1	2.6	2.8	8.2
4	0.9	1.0	0.1	1.7	1.9	5.5
5	1.2	0.9	0.1	2.9	3.4	8.5
6	1.6	1.2	0.3	2.6	2.4	7.9
7	1.5	1.0	0.1	2.3	2.6	7.5
8	2.1	1.6	0.2	3.0	3.3	10.2
9	0.5	1.1	ND <sup>a</sup>	2.3	2.9	6.7
10	0.6	0.8	ND	1.6	1.2	4.3
11	1.0	1.2	0.1	2.5	2.3	7.1
12	1.4	1.4	0.1	3.9	3.8	10.6

<sup>a</sup> ND = not detected.

A statistical analysis of these results is summarized in Table 5. As can be seen, three factors: lignin concentration in water, stirring rate, and reaction time had no significant effect on the results. On the other hand, the Cu dopant concentration had a significant effect on almost all groups of products. The yield of guaiacols was higher at the lower, 5 wt% copper concentration. The only factor with a significant effect on the production of guaiacyl acids was dopant concentration while for the production of syringol and homovanilyl alcohol, a 1.5 lignin-to-catalyst ratio at the 5 wt% Cu concentration yielded the highest concentrations.

These trends are consistent with the catalyst characterization, as the application of 5 wt% Cu led to the formation of fine particles whereas the application of 10% Cu resulted in coagulates, which may clog the pores of the catalyst support and limit the access of phenolic dimers to the active acid sites.

For lignin degradation purposes, Cu doping increased the selectivity of the silica-alumina support toward monomeric compounds. The results also showed that 5 wt% Cu doped silica-alumina was the best option for formation of guaiacols and guaiacyl acids. Previous work indicates that guaiacols may be obtained from the degradation of phenolic dimers [31]. This suggests that the metal dopant only facilitates secondary reactions, since dimers should be more prevalent when the decomposition is less complete.

**Table 5.** A summary of the significance of each factor discovered in the Plackett-Burman screening study.

	Catalyst support type	Dopant used	Lignin concentration in water	LCR	Stirring rate	Dopant concentration	Reaction time
Guaiacols	*	+	*	-	*	-	*
Guaiacyl carbonyl	*	+	*	*	*	*	*
Guaiacyl dimers	+	-	*	*	*	-	*
Guaiacyl acids	*	*	*	*	*	-	*
Others	*	+	*	-	*	-	*
Total GC-elutable compounds	*	+	*	*	*	-	*

“+” indicates the significance of the factor at its high level, “-” indicates the significance of the factor at its low level, “\*” indicates no effect; the levels are shown in Table 2.

The intrinsic activity of the catalyst supports was low due to the limited number of Brønsted acid sites, which may explain why the type of the catalyst support chosen was not as important as other investigated factors from the screening study results. However, in the case of guaiacyl dimers, the silica-alumina catalyst support was shown to have a significant effect. It is possible that the silica-alumina targets the remaining  $\beta$ -O-4 and other ether bonds in Kraft lignin but is less likely to break the stronger C-C bonds due to its low acidity, leading to the production of guaiacyl dimers. This assumption is corroborated by the observed greater concentration of guaiacols in the products from the silica-alumina catalyst support experiments compared to those obtained with  $\gamma$ -alumina catalyst support. As such, it appears that the differences between the two catalysts was primarily in the increased specificity of the silica-alumina catalyst for ether bonds. However, since ether bonds represent only a minor portion of Kraft lignin [1–5], overall lignin conversion into GC-able products was similar for the two catalyst types studied.

### 3.3. Reaction temperature variation study results

The effect of reaction temperature on degradation of lignin was examined in more detail by conducting experiments at three reaction temperatures using the best set of conditions from the initial screening study, as summarized in Table 3. Figure 4 shows the results obtained from GC-MS analysis of the extracted samples in DCM. The overall recovery of liquid phase products was bounded by the temperature region. By increasing the temperature, the concentration of guaiacols and phenol were increased while guaiacyl carbonyls decreased most likely due to dimer instability at higher temperatures. Less expected was the observation that guaiacyl acids as well as total GC elutable compounds showed a bell shaped profile with temperature increase with the maximum concentration at 320 °C.

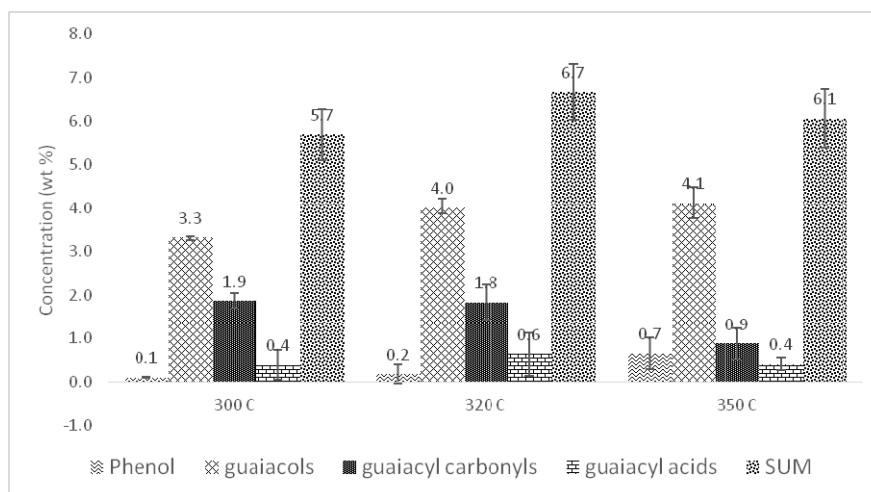


**Figure 4.** The concentration of key groups of product compounds from the reaction temperature study, mass of product per mass of lignin in the original feedstock (wt%).

Thermogravimetric and mass loss curves were obtained at different thermal steps as summarized in Figure 5 and Table 6. As can be seen, the total mass loss decreased with increasing reaction temperature. The weight loss at 25–200 °C can be attributed to monomeric compounds and physically adsorbed water while thermal decomposition of oligomers takes place at 600–900 °C. Since catalytic decomposition of lignin at 350 °C yielded the lowest mass loss in TG analysis, lignin degradation was expected to be more efficient at that temperature. However, GC-MS analysis results showed that a reaction temperature of 320 °C yielded a similar if not higher concentration of low molecular weight compounds, see Figure 4. This suggests that at 350 °C, a greater degree of re-polymerization occurs, which results in a higher yield of coke at the expense of gaseous product formation.

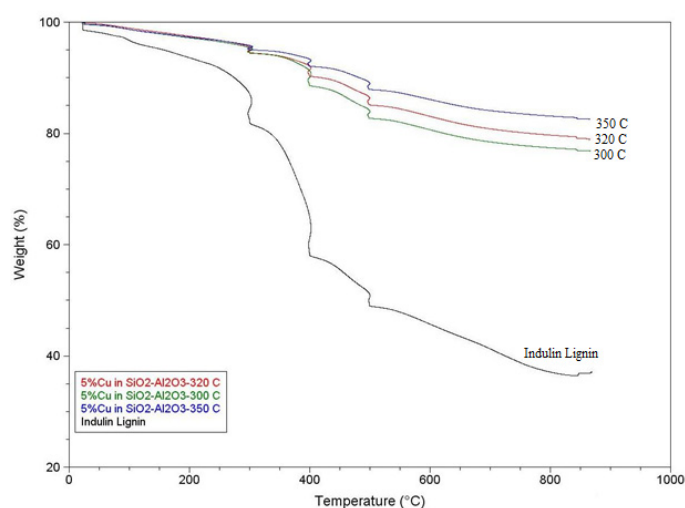


**Figure 5.** Thermogravimetric curves of reactor residues from the reaction temperature study with 5 wt% Cu in SiO<sub>2</sub>/Al<sub>2</sub>O<sub>3</sub> at 300, 320 and 350 °C.

**Table 6.** The temperature profile of mass loss (wt%) obtained by TG analysis of the solid residues recovered from the reactor in the temperature variation study.

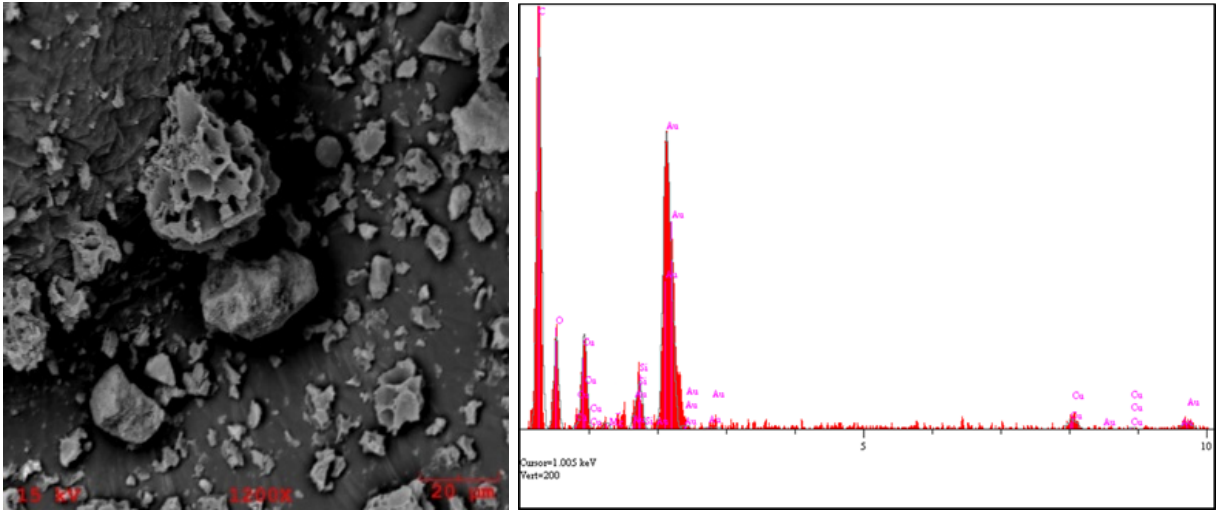
Sample	25–200 °C	200–400 °C	400–600 °C	600–900 °C
Raw Lignin	6.3	28.7	19.2	8.8
5%Cu in SiO <sub>2</sub> -Al <sub>2</sub> O <sub>3</sub> —300 °C	2.8	5.9	10.6	3.8
5%Cu in SiO <sub>2</sub> -Al <sub>2</sub> O <sub>3</sub> —320 °C	2.5	5.4	9.0	4.0
5%Cu in SiO <sub>2</sub> -Al <sub>2</sub> O <sub>3</sub> —350 °C	2.7	4.0	7.2	3.5

This trend reaches its logical conclusion at 400 °C where no detectable mass loss occurs, i.e., virtually no gas phase products are produced (results not shown). This observation is unusual and specific to lignin because in general a greater gas phase product yield is expected at higher temperatures. Lignin's fairly unique propensity to polymerize is well known. However, it is still unusual that it appears to suppress the natural tendency of complex organic substances to form higher concentrations of lighter, gas phase compounds at higher temperatures.

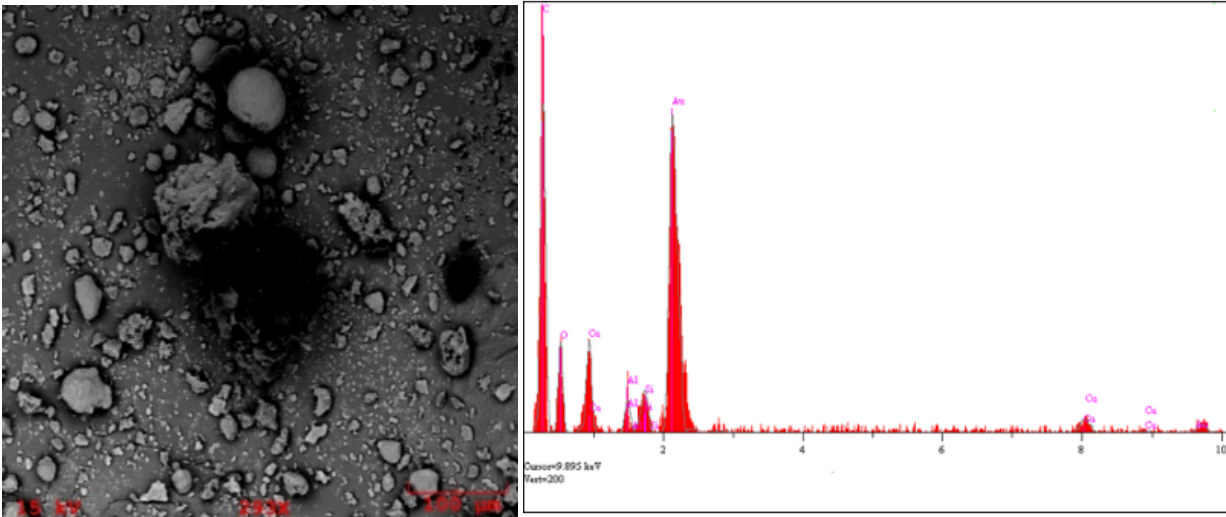
The results suggest that lower reaction temperatures (300 °C) result in more unreacted lignin while higher temperatures (>350 °C) lead to an increased formation of liquid phase products, although at the expense of increased char formation. However, the combined yield of monomer phenolic products was low (~5–7% as shown in Figure 4) and statistically independent of temperature and other operational parameters, although the yields of different chemicals varied with temperature. Consistent with the observed bell-shaped temperature profile of the total GC-able product yield, two trends appear to compete, one being the enhancement of decomposition reactions, and the other, presumably more prominent, being the acceleration of polymerization reactions.

These conclusions were confirmed by SEM analyses of solid residues, which are presented in Figure 6. The morphology of the particles showed differences as the catalyst particles are covered with char. Corroborating this observation, the EDS analysis showed large peaks of elemental carbon in all samples. A comparison of particles obtained at different reaction temperatures shows a trend. At the lowest reaction temperature studied, 300 °C, the char covered catalyst particles are rather porous and have a beehive structure. This observation is consistent with the observed higher yield of phenolic dimers at this temperature, as larger-size dimeric compounds can still access the active surface of the catalyst. Particles obtained at a higher reaction temperature, 320 °C, are not as porous, yet the spherical shape of the catalyst particle is still visible. Char extensively covers the particles and no spherical structure is visible for samples from the 350 °C experiments.

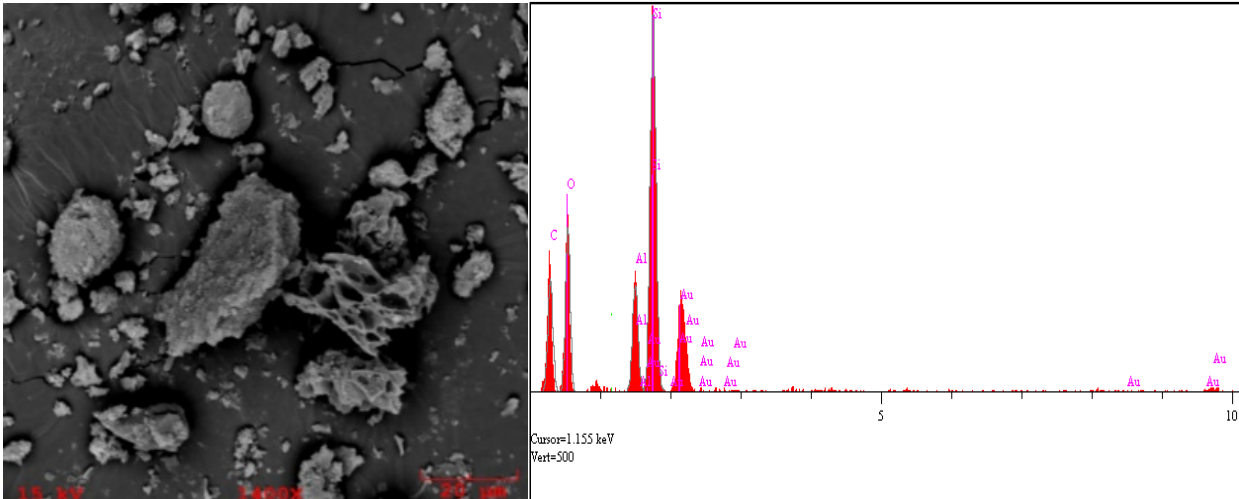
Combining the SEM observations with the results from the GC-MS analysis of the liquid phase products, we can conclude that even at the lowest reaction temperature, 320 °C, the density of char around the silica-alumina catalyst particles is already so high that running the experiments at higher temperatures will not improve catalytic degradation since access to the active sites on the catalyst surface is extremely limited. Therefore, the maximum potential for a Cu doped silica-alumina catalyst can be obtained only at the lowest temperature above the threshold of catalyst activation, i.e., 320 °C, which appears to be suboptimal for this catalyst type.



(a)



(b)



(c)

**Figure 6.** SEM and EDS analysis of solid residues collected from reactor at reaction temperatures of a) 300 °C, b) 320 °C, and c) 350 °C.

## 4. Conclusions

A series of experiments were conducted to explore the use of larger pore, metal doped catalysts to facilitate the decomposition of lignin into more valuable chemical intermediates. The screening study results showed that the dopant concentration had a significant effect on almost all groups of lignin degradation products. Slightly better, though statistically insignificant results were obtained using an amorphous silica-alumina catalyst support than a comparable  $\gamma$ -alumina. Within the parameter bounds of this study, lignin concentration in an aqueous solvent, stirring rate, and reaction time had no major effect on the liquid-phase products distribution.

Studies to examine the effects of reaction temperature on decomposition showed that at 320 °C the formation of monomeric compounds was maximized while the formation of char was minimized. Based on these results, reaction at higher temperature appears to lead to re-polymerization. This effect appears to be significantly enhanced even by incremental increases in temperature. This re-polymerization decreases the monomeric compounds concentration and increases the possibility of char, i.e., cross-linked polymer products formation. Coke deposition appears to be an inherent problem of all catalysts consisting of an alumina-silica support matrix during lignin decomposition, not just zeolites.

Decomposition results from this work were not appreciably better than those previously reported with smaller pore Si-Al catalysts, indicating that the postulate that larger pore catalysts may improve primary decomposition reaction rates may not be correct, apparently due to the overwhelming, unanticipated polymerization effect. The search for efficient catalysts for this process should thus focus on finding catalysts with a lower temperature threshold so that coke deposition is inhibited. Perhaps if such a catalyst is found, larger pore sizes may then improve performance.

## Acknowledgments

We would like to acknowledge support from the National Science Foundation (NSF) via two ND EPSCoR programs: DakotaBioCon IIA-1330842 and CSMS IIA-1355466. Support for REU students involved in the research was provided through the NSF REU Chem: 1460825. Any opinions, findings, and conclusions or recommendations expressed in this material are those of the author(s) and do not necessarily reflect the views of the NSF or ND EPSCoR.

The authors also acknowledge the contributions of Xiadong Hou and the University of North Dakota Institute for Energy Studies for assistance and resources used for SEM and XRD characterization work as well as Alena Kubátová, University of North Dakota Department of Chemistry for assistance and resources used for analytical characterization activities.

## Conflict of interest

All authors declare no conflicts of interest in this paper.

## References

1. Constant S, Wienk HLJ, Frissen AE, et al. (2016) New insights into the structure and composition of technical lignins: A comparative characterisation study. *Green Chem* 18: 2651–2665.

2. Crestini C, Lange H, Sette M, et al. (2017) On the structure of softwood kraft lignin. *Green Chem* 19: 4104–4121.
3. Deuss PJ, Lancefield CS, Narani A, et al. (2017) Phenolic acetals from lignins of varying compositions via iron(III) triflate catalyzed depolymerization. *Green Chem* 19: 2774–2782.
4. Lancefield CS, Wienk HLJ, Boelens R, et al. (2018) Identification of a diagnostic structural motif reveals a new reaction intermediate and condensation pathway in kraft lignin formation. *Chem Sci* 9: 6348–6360.
5. Hita I, Heeres HJ, Deuss PJ (2018) Insight into structure—reactivity relationships for the iron-catalyzed hydrotreatment of technical lignins. *Bioresour Technol* 267: 93–101.
6. Xu C, Arancon R, Labidi J, et al. (2014) Lignin depolymerisation strategies: Towards valuable chemicals and fuels. *Chem Soc Rev* 43: 7485–7500.
7. Asina F, Brzonova I, Kozliak E, et al. (2017) Microbial treatment of industrial lignin: Successes, problems and challenges. *Renew Sust Energ Rev* 77: 1179–1205.
8. Kozliak E, Kubatova A, Artemyeva A, et al. (2016) Thermal liquefaction of lignin to aromatics: Efficiency, selectivity, and product analysis. *ACS Sust Chem Eng* 4: 5106–5122.
9. Chang H, Allan G (1971) Oxidation, Lignins: Occurrence, formation and reactions. Wiley, 433–485.
10. Brebu M, Vasile C (2010) Thermal degradation of lignin—a review. *Cellul Chem Technol* 44: 353.
11. Jae J, Tompsett G, Foster A, et al. (2011) Investigation into the shape selectivity of zeolite catalysts for biomass conversion. *J Catal* 279: 257–268.
12. Xie Z, Liu Z, Wang Y, et al. (2010) An overview of recent development in composite catalysts from porous materials for various reactions and processes. *Int J Mol Sci* 11: 2152–2187.
13. Numan-Al-Mobin A, Voeller A, Bilek H, et al. (2016) Selective synthesis of phenolic compounds from alkali lignin in a mixture of sub- and supercritical fluids: Catalysis by CO<sub>2</sub>. *Energ Fuel* 30: 2137–2143.
14. Yoshikawa T, Yagi T, Shinohara S, et al. (2013) Production of phenols from lignin via depolymerization and catalytic cracking. *Fuel Process Technol* 108: 69–75.
15. Yu Y, Li X, Su L, et al. (2012) The role of shape selectivity in catalytic fast pyrolysis of lignin with zeolite catalysts. *Appl Catal A* 447–448: 115–123.
16. Zheng Y, Chen D, Zhu X (2013) Aromatic hydrocarbon production by the online catalytic cracking of lignin fast pyrolysis vapors using Mo<sub>2</sub>N/γ-Al<sub>2</sub>O<sub>3</sub>. *J Anal Appl Pyrol* 104: 514–520.
17. Li X, Su L, Wang Y, et al. (2012) Catalytic fast pyrolysis of Kraft lignin with HZSM-5 zeolite for producing aromatic hydrocarbons. *Front Environ Sci Eng* 6: 295–303.
18. Liguori L, Barth T (2011) Palladium-Nafion SAC-13 catalysed depolymerisation of lignin to phenols in formic acid and water. *J Anal Appl Pyrol* 92: 477–484.
19. Nguyen T, Maschietti M, Belkheiri T, et al. (2014) Catalytic depolymerisation and conversion of Kraft lignin into liquid products using near-critical water. *J Supercrit Fluid* 86: 67–75.
20. Joffres B, Lorentz C, Vidalie M, et al. (2014) Catalytic hydroconversion of a wheat straw soda lignin: Characterization of the products and the lignin residue. *Appl Catal B* 145: 167–176.
21. Oasmaa A, Johansson A (1993) Catalytic hydrotreating of lignin with water-soluble molybdenum catalyst. *Energ Fuel* 7: 426–429.
22. Yu Z, Li S, Wang Q, et al. (2011) Brønsted/Lewis acid synergy in H-ZSM-5 and H-MOR zeolites studied by <sup>1</sup>H and <sup>27</sup>Al DQ-MAS solid-state NMR spectroscopy. *J Phys Chem C* 115: 22320–22327.

23. Ennaert T, Van Aelst J, Dijkmans J, et al. (2016) Potential and challenges of zeolite chemistry in the catalytic conversion of biomass. *Chem Soc Rev* 45: 584–611.
24. Wua Q, Maa L, Longb J, et al. (2016) Depolymerization of organosolv lignin over silica-alumina catalysts. *Chin J Chem Phys* 29: 474–480.
25. Scherzer J, Gruia A (1996) Hydrocracking science and technology. CRC Press.
26. Hensen E, Poduval D, Degirmenci V, et al. (2012) Acidity characterization of amorphous silica-alumina. *J Phys Chem C* 116: 21416–21429.
27. Van Borm R, Aerts A, Reyniers M, et al. (2010) Catalytic cracking of 2, 2, 4-trimethylpentane on FAU, MFI, and bimodal porous materials: Influence of acid properties and pore topology. *Ind Eng Chem Res* 49: 6815–6823.
28. Yu Y, Li X, Su L, et al. (2012) The role of shape selectivity in catalytic fast pyrolysis of lignin with zeolite catalysts. *Appl Catal A* 447–448: 115–123.
29. Voeller K, Bilek H, Kreft J, et al. (2017) Thermal carbon analysis enabling comprehensive characterization of lignin and its degradation products. *ACS Sust Chem Eng* 5: 10334–10341.
30. Pourjafar S (2017) An Investigation of the Thermal Degradation of Lignin. Doctoral dissertation, University of North Dakota, USA.
31. Wua Q, Maa L, Longb J, et al. (2016) Depolymerization of organosolv lignin over silica-alumina catalysts. *Chin J Chem Phys* 29: 474–480.



**AIMS Press**

© 2018 the Author(s), licensee AIMS Press. This is an open access article distributed under the terms of the Creative Commons Attribution License (<http://creativecommons.org/licenses/by/4.0>)